Dalton Transactions

ROYAL SOCIETY OF CHEMISTRY

PAPER

View Article Online
View Journal | View Issue

Cite this: *Dalton Trans.*, 2024, **53**, 9452

Dinuclear group IV metal complexes based on a bis(indenyl)-(*E*/*Z*)-stilbene platform: a potential prototype of "photoswitchable" catalysts for olefin polymerization†

Nuria Romero, ‡[a] Thierry Chavagnan,‡[a] Thierry Roisnel, [b] Alexandre Welle,[c] Evgueni Kirillov *[a] and Jean-François Carpentier *[a]

The preparation of dizirconium complexes based on a novel bis(indenyl)-(*E*/*Z*)-stilbene platform was explored. Negishi coupling between the *in situ*-generated diorganozincates obtained from the respective *o*/*m*/*p*-(*E*/*Z*)-dibromostilbenes and the bromo-functionalized zirconocene (η^5-Cp*)(η^5-2-methyl-4-bromoindenyl)$ZrCl_2$, or, alternatively, the preparation of bis(indene)stilbene pro-ligands {*o*/*m*/*p*-(*E*/*Z*)-BisIndSB}H_2 through Negishi coupling of the corresponding dibromostilbenes with 4-bromoindene and subsequent metallation/transmetallation with Cp*$ZrCl_3$ or $Zr(NMe_2)_4$, allowed the preparation of a series of dinuclear complexes. These were analyzed by NMR spectroscopy and some of them by iASAP-mass spectrometry and by X-ray diffraction studies. Experimental results were compared with DFT modelling of the targeted dinuclear complexes evidencing that the (*E*)-complexes are more stable by 7–11 kcal mol^{-1} than their (*Z*)-analogues. Thermal, uncontrolled isomerization of (*Z*)- to (*E*)-stilbene platform was observed experimentally for some systems, in the course of their synthesis, either from the (*Z*)-dibromostilbene reagent or on the dinuclear complexes resulting from the Negishi coupling. Photoisomerization of the (*E*)- and (*Z*)-{BisIndSB}H_2 proligands and of complexes {*o*-(*E*)-BisIndSB}$(Zr(NMe_2)_3)_2$ and {*m*-(*E*)-BisIndSB}$(ZrCl_2Cp^*)_2$ was investigated under a variety of conditions. It proved effective for the proligands but induced decomposition of the dizirconium complexes. Time-dependent DFT (TD-DFT) computations were performed to identify unambiguously the nature of the observed absorption bands and account for decomposition of the complexes. Preliminary ethylene/1-hexene homo- and copolymerization investigations did not evidence putative cooperativity phenomena within these dinuclear systems nor significantly differentiated behavior between the (*Z*)- and (*E*)-isomers of a given type of complex under the reaction conditions investigated.

Received 20th February 2024,
Accepted 13th May 2024

DOI: 10.1039/d4dt00498a

rsc.li/dalton

Introduction

Molecular switches are chemical compounds that can be reversibly interconverted in a controlled fashion, upon action of an external stimulus, between at least two states, each displaying unique properties.[1] These two states may differ in quite various aspects: atom connectivity and geometry (formation or breaking of bonds), spatial configuration (*e.g.*, transformation of one stereoisomer into another) or conformation, or oxidation state of a redox-active element. As a result, the two states may exhibit quite different chemical and physico-chemical properties. Switching the property, function, and activity of a molecule with simple chemico-physical stimuli (acid/base, metal ion, redox, light, sound, electric potential or mechanical force) is possible only through judicious incorporation of a reversibly responsive regulatory feature. More and more examples of molecular switches applicable to catalysis, exploit-

[a]*Univ Rennes, CNRS, ISCR (Institut des Sciences Chimiques de Rennes), UMR 6226, F-35000 Rennes, France. E-mail: evgueni.kirillov@univ-rennes.fr, jean-francois.carpentier@univ-rennes.fr*
[b]*Univ Rennes, CNRS, Centre de diffractométrie, ISCR (Institut des Sciences Chimiques de Rennes), UMR 6226, F-35000 Rennes, France*
[c]*TotalEnergies OneTech Belgium, Zone Industrielle C, B-7181 Feluy, Belgium*

†Electronic supplementary information (ESI) available: NMR spectra of organic compounds and complexes, mass spectra for complexes {*o*-(*E*/*Z*)-BisIndSB}$(Zr(NMe_2)_3)_2$, experimental absorption spectra and TD-DFT calculated absorption spectra of proligands and (*Z*)- and (*E*)-{*o*-BisIndSB}$(Zr(NMe_2)_3)_2$ complexes, ORTEP plots and crystallographic data, polymerization data, representative DSC and SEC traces of polyethylene and ethylene/1-hexene copolymer samples. CCDC 1894661–1894663 and 2322679–2322683. For ESI and crystallographic data in CIF or other electronic format see DOI: https://doi.org/10.1039/d4dt00498a

‡Those two authors contributed equally to this manuscript.

ing differences in chemical reactivity between the two states of a catalyst, have been described in the literature.[2] In the field of switchable polymerization catalysis,[3] landmark reports have concerned the ring-opening metathesis polymerization (ROMP) of cycloolefins[4] and atom-transfer radical polymerization (ATRP) of (meth)acrylates,[5] but most examples have concerned the ring-opening polymerization (ROP) of cyclic esters using essentially redox chemoswitchable but also photoswitchable metal-based catalysts.[6–11] Examples of allosteric control by non-redox chemical switching of a metal-based catalyst[12] or using photoswitchable organocatalysts[13] have also been reported. In the case of Ziegler–Natta type olefin polymerization, the use of such switchable catalyst systems is still limited;[14] it may allow for selective comonomer discrimination and may give rise to new classes of polymeric materials with sophisticated microstructures and valuable properties.

On the other hand, homobimetallic systems with short and long metal–metal distances are receiving increased attention because of possible 'cooperative effects', in which the use of multimetallic complexes show clear enhancement of catalytic outcomes when compared with the sum of their corresponding mononuclear counterparts.[15] Several such examples of cooperativity have been claimed with bimetallic systems for olefin polymerization.[16–19]

To our knowledge, the combination of switchable platforms with bimetallic systems remains scarce. In this work, we aimed at exploring the possibility to develop new homodinuclear group IV metallocene complexes based on the simple stilbene (SB) platform. Indeed, stilbene is a molecule which allows easy functionalization at the phenyl rings, hence enabling installation of suitable coordination environment for stabilizing group IV metals. It is also a platform which is readily prone to *Z*/*E* isomerization of the C=C bond and thus to possible photoswitch[1,20] of the dinuclear (pre)catalyst in between two different configurations; this would allow varying the intermetallic distances between the catalytic centers, with possible distinctive catalytic behavior in the two states, including possible catalytic cooperativity. Herein we present computational and experimental results towards the design, synthesis and analysis of a variety of novel bis(indenyl-zirconocene)s based on such a photoswitchable stilbene platform (Fig. 1).

Results and discussion

DFT-modelling of targeted dinuclear complexes

The different targeted compounds were first computed by DFT to assess their relative free energies (Fig. 2; see the Experimental section for computational details). In all cases, expectedly, the optimized geometries of the complexes with a (*E*)-configurated stilbene platform were found more stable by 7–11 kcal mol^{-1} than their (*Z*)-analogues; this reflects essentially the difference in stability of the (*E*)- *vs.* (*Z*)-stilbene platform itself.[21] Consistently, rather minimal differences (<3 kcal mol^{-1}, *i.e.* beyond accuracy of the DFT method) were computed between the two diastereomers of a given compound, as determined by the relative planar chirality at both metallocene sites (for instance, for (*E*)- and (*Z*)-{*m*-BisIndSB}($ZrCl_2Cp^*$)$_2$, ΔE(dia#1 *vs.* dia#2) = 2.4 and 2.3 kcal mol^{-1}, respectively). Also, for all complexes, the energy surfaces were rather flat and hence there is a large variety of 'energetically accessible' conformers with Zr···Zr distances varying over a broad range; for instance, for (*E*)- and (*Z*)-{*o*-BisIndSB}($ZrCl_2Cp^*$)$_2$ conformers differing only by 2 kcal mol^{-1}, the computed Zr···Zr distances are in the 8.8–11.2 Å and 7.8–12.1 Å ranges, respectively.

Synthetic strategies towards bis(indenyl-zirconocene)s based on a stilbene platform

We next explored synthetic pathways towards these dinuclear Zr complexes, starting from dibromostilbenes as precursors. As described in the literature,[22–24] 3,3′-dibromostilbene can be readily prepared by Wittig reaction as a *Z*/*E* mixture from *m*-bromobenzyl bromide and *m*-bromobenzaldehyde, and both stereoisomers can be separated eventually by flash column chromatography. (*Z*)- and (*E*)-2,2′-dibromostilbenes were prepared following similar synthetic protocols.[25] The solid-state crystal structures of (*E*)-3,3′-, (*Z*)- and (*E*)-2,2′-dibromostilbenes were determined by X-ray diffraction (see Fig. S1–S3 and Table S1 in the ESI†). (*Z*)-4,4′-Dibromostilbene was also obtained by Wittig coupling while the (*E*)-isomer was synthetized by McMurry coupling.[26]

The synthesis of the dinuclear bis(indenyl-Cp*) zirconium complexes, {*o*/*m*/*p*-(*E*/*Z*)-BisIndSB}($ZrCl_2Cp^*$)$_2$, was then attempted following two distinct routes, differing in the reactions sequence (Scheme 1): (a) Negishi coupling between the *in situ*-generated diorganozincates obtained from the respective *o*/*m*/*p*-(*E*/*Z*)-dibromostilbenes and the bromoindenyl-functionalized zirconocene complex (η^5-pentamethylcyclopentadienyl) (η^5-2-methyl-4-bromoindenyl)$ZrCl_2$;[27] (b) the preparation of bis(indene)stilbene pro-ligands {*o*-(*E*/*Z*)-BisIndSB}H_2 through Negishi coupling of the corresponding dibromostilbenes with 4-bromoindene and subsequent metallation/transmetallation with Cp^*ZrCl_3.

Use of **route A** starting from *o*-(*Z*)- and *o*-(*E*)-dibromostilbenes, under different reaction conditions, did not prove quite effective. The NMR spectroscopic data of the yellow solid material recovered from the Negishi coupling from the *o*-(*Z*)-platform, despite 3–4 successive recrystallizations from toluene/pentane solutions, were complicated and not conclusive about the purity of the targeted {*o*-(*Z*)-BisIndSB}($ZrCl_2Cp^*$)$_2$.§ In the aliphatic region of the ^{1}H NMR spectrum (Fig. S10†), six signals were observed for the Cp* groups and four signals corresponding to the methyl groups of the indenyl moiety. These observations suggest that the product isolated is possibly composed of a mixture of diastereomers of *E*/*Z*-stereoisomers of the targeted complex.

§ Attempts to record high-resolution mass spectra by iASAP or ESI techniques, to confirm the identity of the complex, failed, as for all {*o*/*m*/*p*-(*E*/*Z*)-BisIndSB}($ZrCl_2Cp^*$)$_2$. iASAP-MS data could be obtained only for {*o*-(*E*/*Z*)-BisIndSB}($Zr(NMe_2)_3$)$_2$ complexes; see the ESI.†

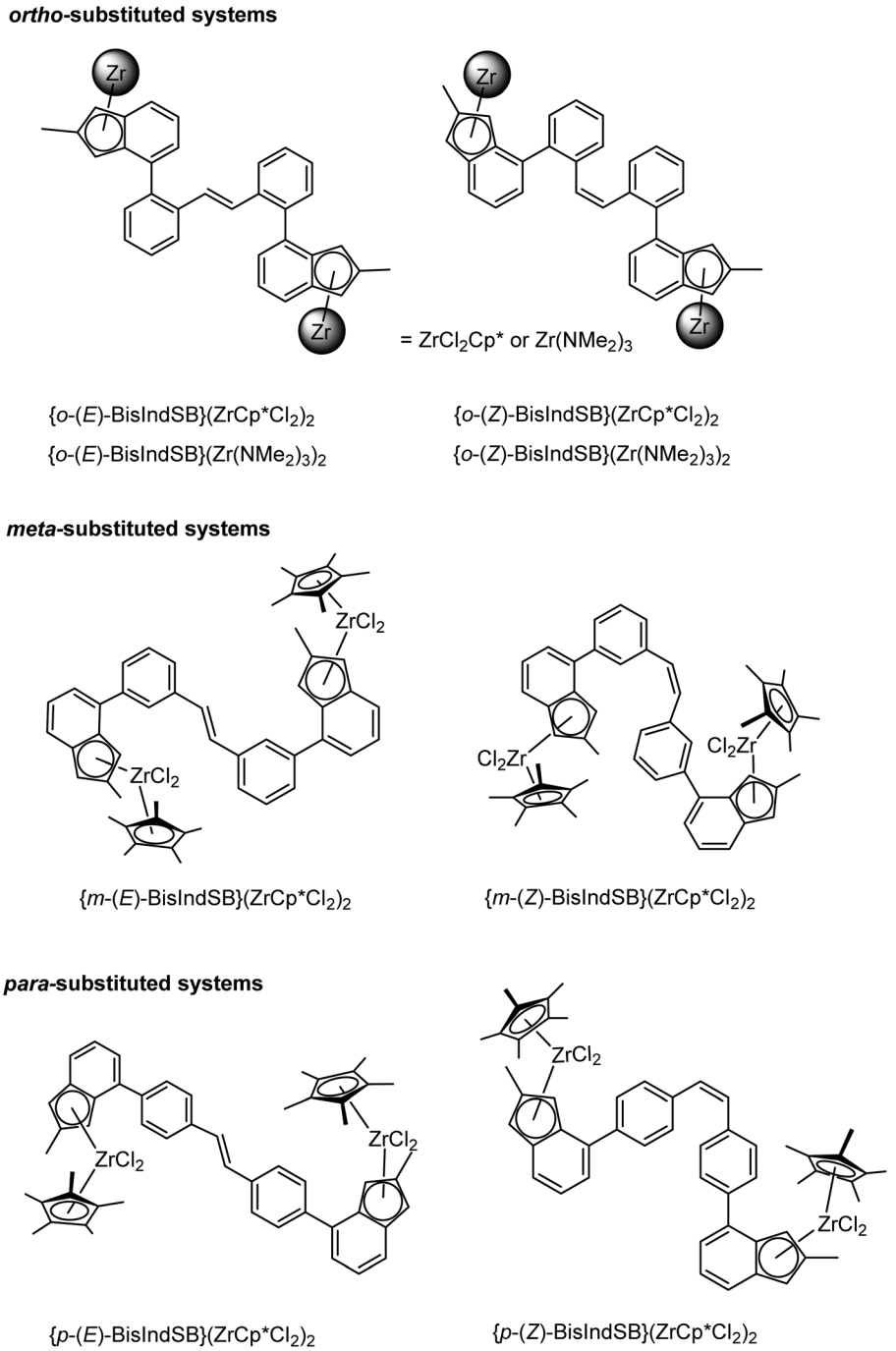

Fig. 1 Targeted dinuclear bis(indenyl-zirconocene)s based on a photoswitchable stilbene platform.

Use of the same **route A** conditions starting from 600 mg of (*E*)-2,2′-dibromostilbene, with several recrystallization steps of the crude reaction product from toluene/pentane and dichloromethane/hexane solutions, yielded only a few crystals of metallocene (*ca.* 5 mg). An X-ray diffraction analysis revealed that, instead of complex {*o*-(*E*)-BisIndSB}($ZrCl_2Cp^*$)$_2$, its (*Z*)-isomer was isolated (Fig. 3). This result is somehow unexpected as {*o*-(*E*)-BisIndSB}($ZrCl_2Cp^*$)$_2$ is calculated to be significantly more thermodynamically stable than the (*Z*)-analogue (see the above DFT computations, Fig. 2, $\Delta G_{(E/Z)} = 11.4$ kcal mol^{-1}). It is possible that crystallization of the (*Z*)-isomer is driven by packing forces. Yet, those NMR and X-ray results evidence that dynamic (*E*) ⇄ (*Z*) isomerization of the stilbene platform takes place in solution under route A conditions, even at ambient temperature. Another isomerization in solution at ambient temperature, yet from the (*Z*)- to the (*E*)-isomer, was observed in the synthesis of {*m*-BisIndSB}($ZrCl_2Cp^*$)$_2$ (*vide infra*). In the asymmetric unit of the solid-state structure of {*o*-(*E*)-BisIndSB}

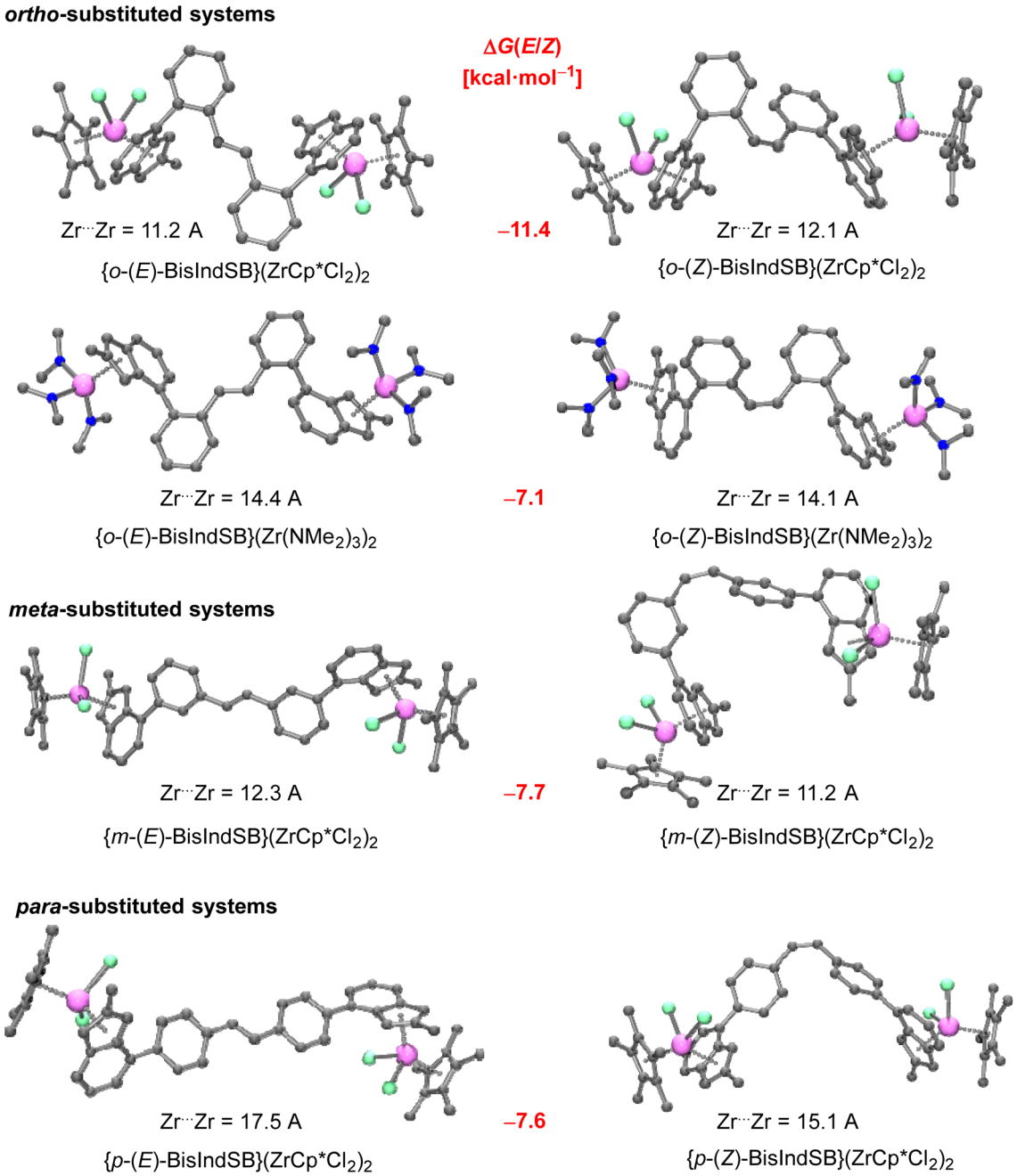

Fig. 2 DFT-optimized (B3PW91/def2-SVP, SMD(toluene)) structures of bis(indenyl-zirconocene)s based on a photoswitchable stilbene platform, with the corresponding computed Zr···Zr distances (in Å) and relative free energies (in kcal mol^{-1}); for each compound, only one diastereomer, as determined by the relative planar chirality at both metallocene sites, is depicted.

$(ZrCl_2Cp^*)_2$, only one diastereomer is observed (as a racemic). The Zr···Zr distance observed (11.5 Å) is close to that determined in the DFT-optimized molecule (12.1 Å). The torsion angle between the planes of the two phenyl rings of the (*Z*)-stilbene unit is about 8°.

The sequence-reversed synthetic **route B** was explored to access the targeted {*o*-(*E*/*Z*)-BisIndSB}$(ZrCl_2Cp^*)_2$ complexes (Scheme 1). The first step involves the synthesis of {*o*-(*E*/*Z*)-BisIndSB}H_2 proligands, which were independently synthetized in good yields (68–71%) through Negishi coupling of the corresponding (*E*/*Z*)-2,2′-dibromostilbene with 4-bromoindene; their solid-state crystal structures were also determined by X-ray diffraction (see Fig. S8, S9 and Table S1 in the ESI†). No thermal interconversion between the isomers of both proligands was observed in toluene or chloroform solution at room temperature, as confirmed by NMR spectroscopy. The proligands were then metallated with *n*BuLi (2 equiv.) and reacted with Cp^*ZrCl_3 (2 equiv.), following a transmetallation protocol

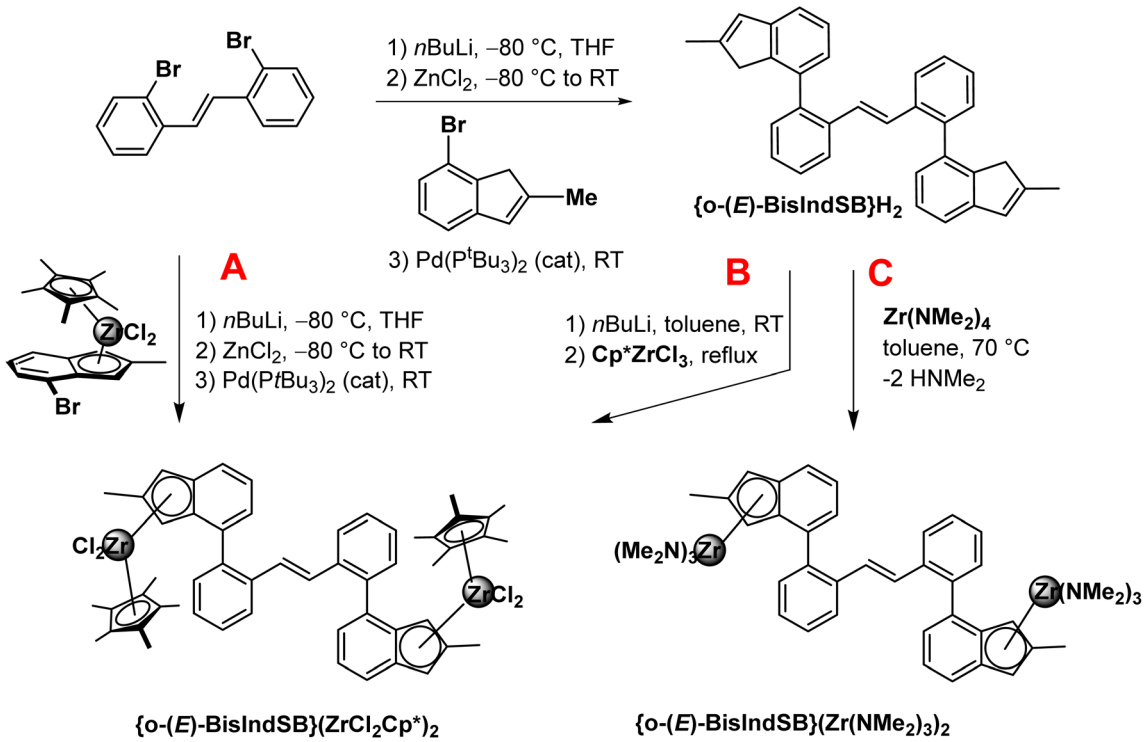

Scheme 1 Synthetic **routes A–C** explored towards dinuclear zirconocenes {*o*/*m*/*p*-(*E*/*Z*)-BisIndSB}$(ZrCl_2Cp^*)_2$ and {*o*-(*E*/*Z*)-BisIndSB}$(Zr(NMe_2)_3)_2$ based on the stilbene platform, as illustrated from (*E*)-2,2′-dibromostilbene.

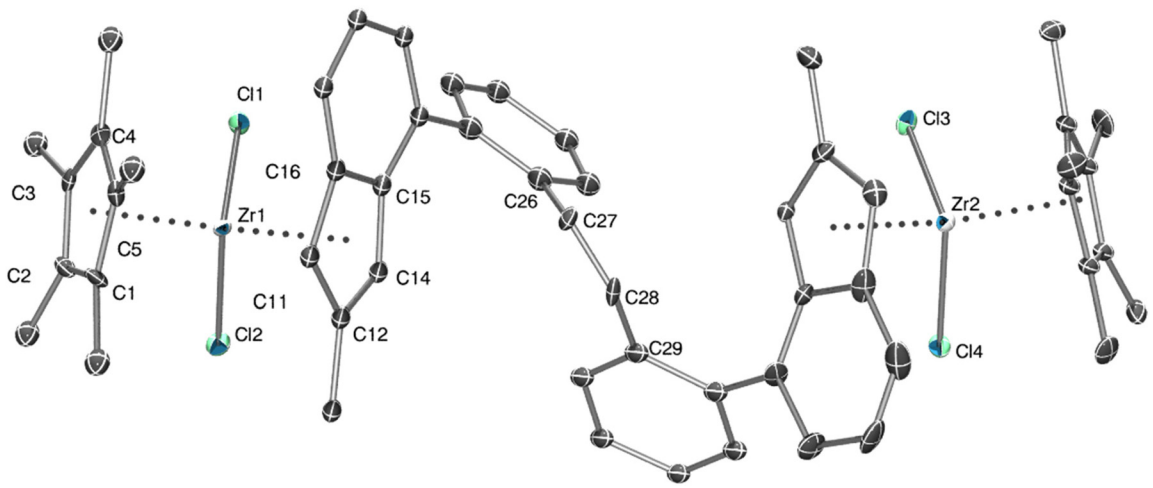

Fig. 3 ORTEP plot of the solid-state molecular structure of {*o*-(*Z*)-BisIndSB}$(ZrCl_2Cp^*)_2$ (ellipsoids set at 50% probability level; all H atoms omitted for clarity). Selected bond distances (Å) and angles (°): Zr(1)–Cp*(centroid), 2.237; Zr(1)–Ind(centroid), 2.235; C(27)–C(28), 1.376(18); Cp*(centroid)–Zr–Ind(centroid), 132.57; C(26)–C(27)–C(28)–C(29), –8(2); Zr(1)/Zr(2) distance, 11.497.

similar to that described for the synthesis of the mononuclear Cp*(η^5-2-methyl-4-bromoindenyl)$ZrCl_2$.[27] Yet, as for **route A**, the NMR spectroscopic data for the thus recovered materials were unclear, even after several recrystallizations of the crude product in toluene/pentane solution, featuring broad, multiple signals. Repeated attempts to obtain crystals of the metallocenes suitable for X-ray analysis failed.

Metallation of the {*o*-(*E*/*Z*)-BisIndSB}H_2 proligands was investigated with other metal precursors. As monitored by ^{1}H NMR spectroscopy in C_6D_6, no reaction occurred with Hf$(CH_2Ph)_4$ (2 equiv.) after heating at 70 °C for 18 h. On the other hand, under the same conditions, effective and selective reaction proceeded with $Zr(NMe_2)_4$ with concomitant amine elimination; the reaction mixture was therefore regularly

stripped under vacuum over a 36 h period to ensure complete reaction. Recrystallization of the final products in toluene/hexane solutions afforded the corresponding complexes {*o*-(*E*/*Z*)-BisIndSB}$(Zr(NMe_2)_3)_2$ in 86% and 78% yield, respectively. Their identity and purity were established by iASAP mass spectrometry (Fig. S33†),[28] and ^{1}H and ^{13}C NMR spectroscopy (see the Experimental section). Characteristic ^{1}H NMR resonances (C_6D_6, 25 °C) for {*o*-(*E*)-{BisIndSB}$(Zr(NMe_2)_3)_2$} (Fig. S25†) include signals at δ_H 2.13, 2.76 ppm for the methyl of the indenyl moiety and the dimethylamido groups, respectively, and at δ 2.14 and 2.76 ppm for the (*Z*)-isomer (Fig. S29†). The solid-state structure of {*o*-(*E*)-{BisIndSB}$(Zr(NMe_2)_3)_2$} was confirmed by a single-crystal X-ray diffraction study (Fig. 4). In the asymmetric unit, only one diastereomer is observed (as a *racemate*), where the two Zr atoms are located on the opposite sides with respect to the plane defined by the (*E*)-stilbene moiety. The distance between the two metal centers is 14.25 Å, very close to the value (14.4 Å) calculated for the DFT-optimized structure (Fig. 2).

The preparation of metallocenes {*m*/*p*-(*Z*/*E*)-BisIndSB}$(ZrCl_2Cp^*)_2$ was investigated *via* **route A**, from the corresponding 3,3′-/4,4′-(*Z*)-/(*E*)-dibromostilbene platforms.

Complex {*m*-(*E*)-BisIndSB}$(ZrCl_2Cp^*)_2$ was thus successfully isolated in 66% yield and characterized by NMR spectroscopy and X-ray crystallography. Informative ^{1}H, ^{13}C{^{1}H}, ^{1}H–^{1}H COSY and ^{1}H–^{13}C HSQC NMR spectra could be recorded (Fig. S11–S14†); yet, the number of resonances in these spectra suggest that, likely, a mixture of diastereomers resulting from planar chirality at the two indenyl moieties is formed. This is expected considering the low energy difference between such two diastereomers as computed by DFT (ΔG(dia#1/dia#2) = 3.1 kcal mol^{-1}, for the (*E*)-isomer; *vide supra*). The solid-state structure features in the unit cell two independent molecules of the same diastereomer, with essentially the same geometric features, where the two Zr atoms are located on the opposite sides with respect to the plane defined by the stilbene moiety (Fig. 5). The Zr···Zr distance observed in the solid state (11.5 Å) is only slightly shorter than that calculated (12.3 Å) for the DFT-optimized structure (Fig. 2).

The preparation of the (*Z*)-analogue, that is {*m*-(*Z*)-BisIndSB}$(ZrCl_2Cp^*)_2$, was attempted using similar conditions. However, ^{1}H, ^{13}C{^{1}H} and ^{1}H–^{13}C HSQC NMR analyses of the resulting crude and recrystallized products (Fig. S15–S18†) revealed what appears to be mixtures of the (*Z*)- and (*E*)-isomers. NMR monitoring indicated that thermal isomerization occurs at two stages at room temperature: from the (*Z*)-3,3′-dibromostilbene reagent, and also on the dinuclear complex resulting from the Negishi coupling. This fact precluded the isolation of pure {*m*-(*Z*)-BisIndSB}$(ZrCl_2Cp^*)_2$.

The preparation of {*p*-(*E*)-BisIndSB}$(ZrCp^*Cl_2)_2$ and {*p*-(*Z*)-BisIndSB}$(ZrCp^*Cl_2)_2$ was undertaken following the same **route A**. Both complexes were isolated in 40% and 58% yield, respectively. ^{1}H, ^{13}C{^{1}H} and ^{1}H–^{13}C HSQC NMR data indicated that the two species were produced without significant isomerization and are rather stable at room temperature in benzene solutions. Yet, no crystal suitable for X-ray diffraction studies could be recovered.

Photoisomerization studies

Photoisomerization of (*E*)- and (*Z*)-{BisIndSB}H_2 proligands was investigated (Scheme 2). The UV-vis spectrum of each compound exhibited two absorption bands at λ_{max} = 257 and 305 nm and λ_{max} = 257 and 310 nm for the (*E*)- and (*Z*)-isomers, respectively (Fig. S34†).

The selective irradiation at λ = 330 nm of a 10^{-5} M dichloromethane solution of (*E*)-{BisIndSB}H_2 was monitored by UV-vis spectrometry (Fig. 6). A decrease of the absorption band at λ = 305 nm was observed and the photostationary state was reached after 80 min. Conversion of (*E*)- to (*Z*)-{BisIndSB}H_2 in CD_2Cl_2 solution at λ = 330 nm was confirmed by ^{1}H NMR spectroscopy *via* monitoring of the hydrogen signal of the indene moiety [(*E*)-, δ_H 6.56 ppm (^4J = 1.6) and (*Z*)-, δ_H 6.51 ppm (^4J = 1.5)] (Fig. S36†). The isomerization reached a photostationary state after 84 h of irradiation with an equilibrium molar ratio

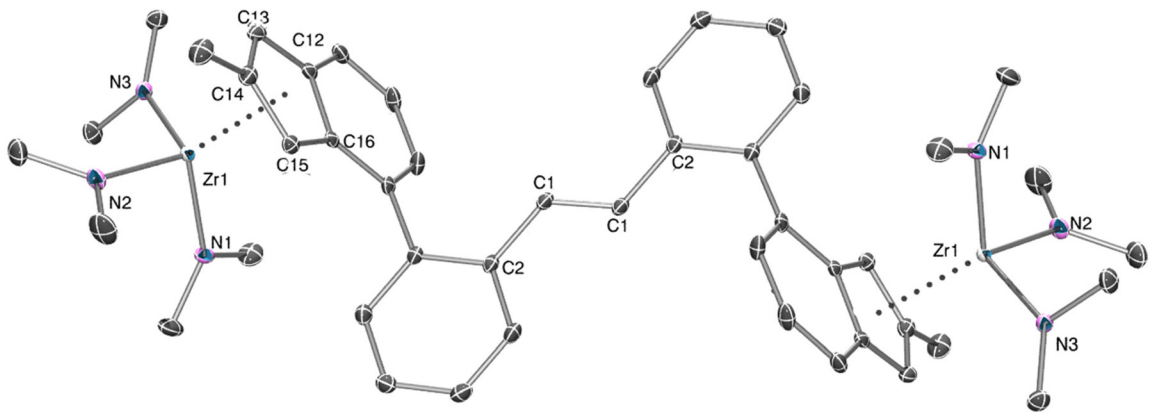

Fig. 4 ORTEP plot of the solid-state molecular structure of {*o*-(*E*)-BisIndSB}$(Zr(NMe_2)_3)_2$ (ellipsoids set at 50% probability level; all H atoms omitted for clarity). Selected bond distances (Å) and angles (°):C(1)–C(1′), 1.340(3); Zr(1)–Ind(centroid), 2.296; N(1)–Zr–Ind(centroid), 119.94; N(2)–Zr–Ind (centroid), 116.02; C(2)–C(1)–C(1′)–C(2′), 180.0; Zr(1)/Zr(1′) distance, 14.251.

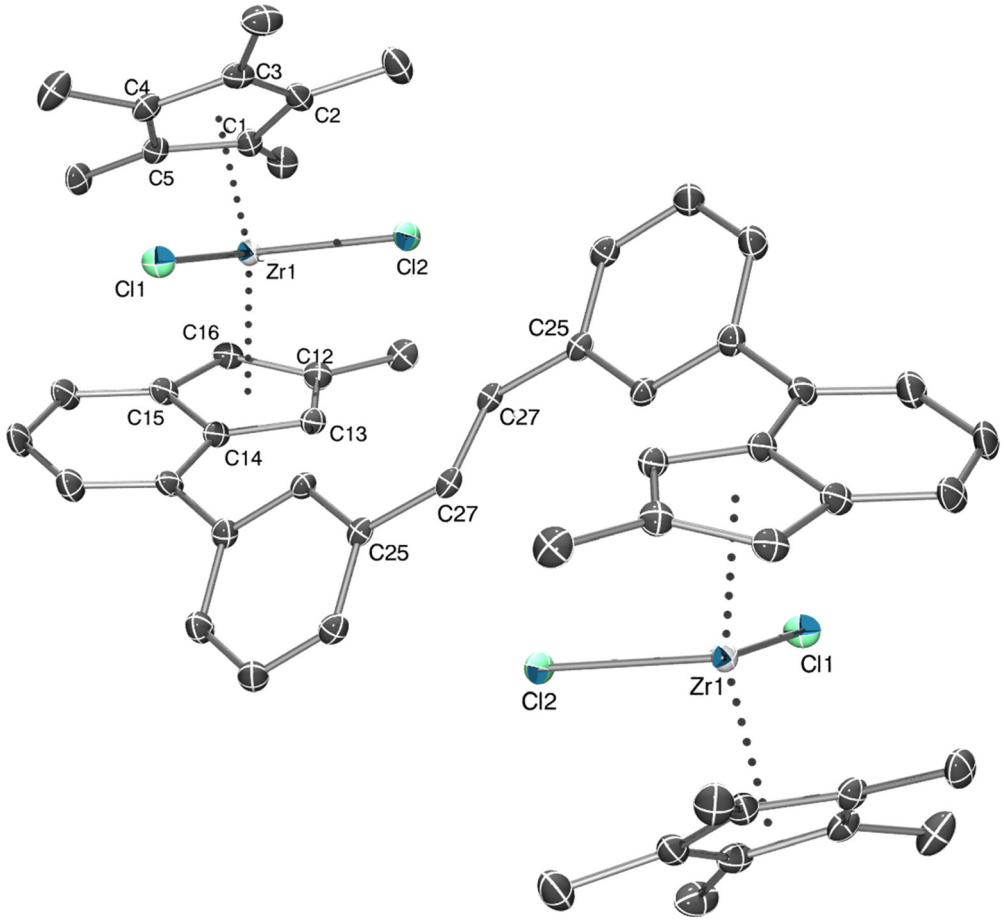

Fig. 5 ORTEP plot of the solid-state molecular structure of {*m*-(*E*)-BisIndSB}($ZrCl_2Cp^*$)$_2$ featuring the two diastereomers (ellipsoids set at 50% probability level; all H atoms omitted for clarity; only one of the two independent molecules shown). Selected bond distances (Å) and angles (°): C(27)–C(27′), 1.338(6); Zr(1)–Cp*(centroid), 2.219; Zr(1)–Ind(centroid), 2.250; Cp*(centroid)–Zr–Ind(centroid), 132.15; C(25)–C(27)–C(27′)–C(25′), 180.0; Zr(1)/Zr(1′) distance, 11.510.

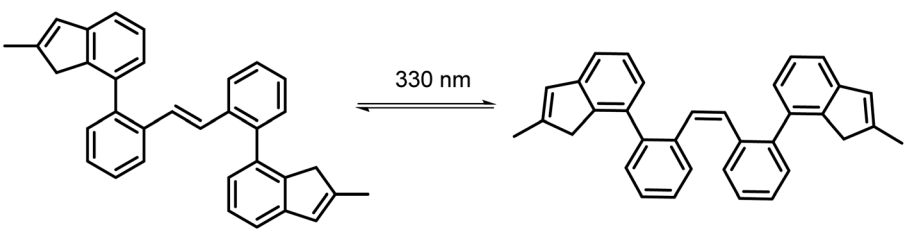

Scheme 2 Photoisomerization of (*E*)- to (*Z*)-{BisIndSB}H_2 proligands by UV irradiation.

E/*Z* of 19 : 81. However, reversible isomerization of (*Z*)- to (*E*)-{BisIndSB}H_2 could not be achieved. Irradiation of a solution of (*Z*)-{BisIndSB}H_2 at λ = 280 nm led to degradation and no further change in the absorption spectra was observed when irradiation was conducted at λ = 350 nm.

The electronic spectra of (*E*)- and (*Z*)-{*o*-BisIndSB}{Zr$(NMe_2)_3$}$_2$ complexes exhibited each a single absorption band at λ_{max} = 294 and 293 nm, respectively (Fig. S37†). Inflection points at λ = 340 nm for {*o*-(*E*)-BisInd}{Zr$(NMe_2)_3$}$_2$ and λ = 325 nm for its (*Z*)-analogue are also observed in the absorption spectra. As for the proligands, photoisomerization of {*o*-(*E*)-BisIndSB}{Zr$(NMe_2)_3$}$_2$ to the (*Z*)-isomer could not be achieved. Direct irradiation of a toluene solution of {*o*-(*E*)-BisIndSB}{Zr$(NMe_2)_3$}$_2$ at λ = 350 nm led to degradation of the complex, inferred by a gradual decrease in intensity of the absorption band (Fig. 7). Similar observations were made upon irradiation at λ = 320 and 350 nm of solutions of {*m*-(*E*)-BisIndSB}($ZrCl_2Cp^*$)$_2$. These results suggest that UV irradiation at λ = 350 nm is already too energetic and may provoke cleavage/decay of the Zr–ligand bonds.

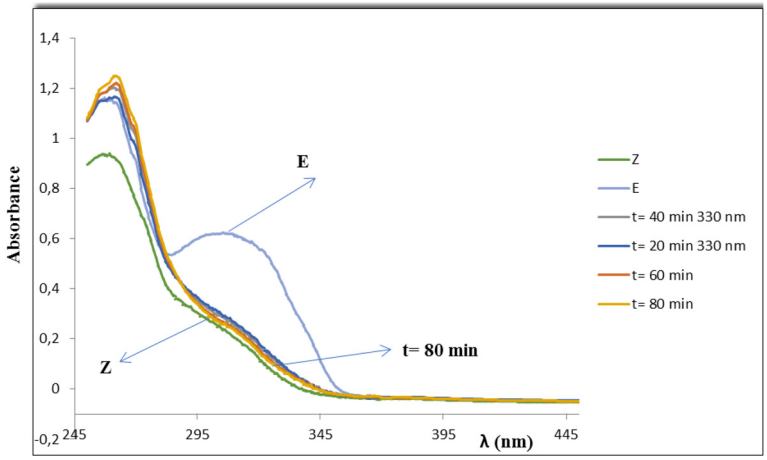

Fig. 6 Photoisomerization of (*E*)- to (*Z*)-{BisIndSB}H_2 proligands.

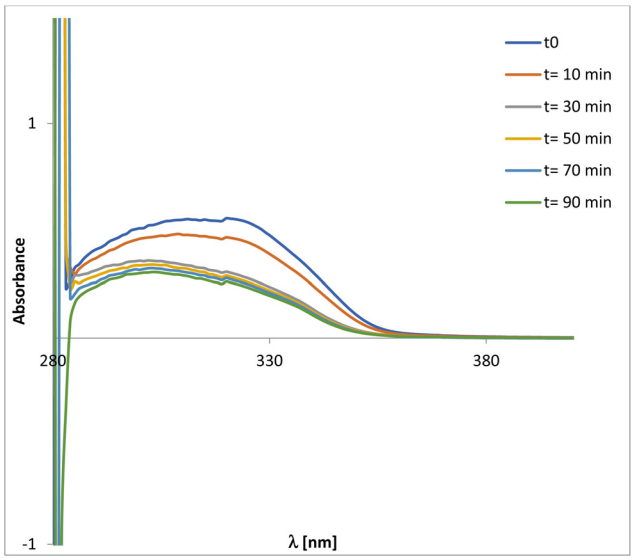

Fig. 7 Photoirradiation of a toluene solution of {*o*-(*E*)-BisIndSB}(Zr$(NMe_2)_3)_2$ at λ = 350 nm.

To prevent degradation of the dinuclear complexes, we explored indirect irradiation using photosensitized stilbene isomerization.[29] Screening of different molecules (fluorene, 9-bromophenanthrene, 2,7-dibromofluorene...) eventually led us to use pyrene as sensitizer. Photoisomerization of proligand (*Z*)-{BisIndSB}H_2 upon irradiation at λ = 330 nm in toluene solution in presence of 1.2 equiv. of pyrene led to 7% conversion to the (*E*)-isomer after 24 h, as monitored by ^{1}H NMR spectroscopy (Fig. S39†). Slow isomerization was also observed at λ = 350 nm (9% conversion after 24 h) (Fig. S40†). These results encouraged us to irradiate at a lower energy (to prevent decomposition of the complexes) using a different sensitizer which would be compatible with our bimetallic system. Yet, no conversion was observed when a solution of {*o*-(*Z*)-BisIndSB}H_2 and perylene (1.2 equiv.) was irradiated at λ = 450 nm for 60 h (as monitored by ^{1}H NMR spectroscopy, Fig. S41†). This implies that this method is not suitable for the photoisomerization of the sensitive bimetallic complexes. Possible alternatives to address this issue involve ligand tuning and/or changing zirconium for another group 4 metal center.

TD-DFT computations

We then sought additional clues on the electronic structure of the above proligands and complexes, and carried out time-dependent DFT (TD-DFT) computations to identify unambiguously the nature of the observed absorption bands (Table 1).[30] The methodology used is provided in the ESI. TD-DFT calculations performed for both proligands (Fig. S35†) returned calculated UV-vis spectra with absorption bands at λ_{max} = 330, 264 and 256 nm for *o*-(*E*)-{BisIndSB}H_2 and at λ_{max} = 319 and 258 nm for the (*Z*)-isomer, consistent with the experimental data.

For *o*-(*E*)-{BisIndSB}H_2, the calculated lower energy absorption band is due to the HOMO → LUMO or π → π* transition. Indeed, the HOMOs and LUMOs are centered on the diarylethene (stilbene) platforms,[30c,d] with 88% and 89% contributions, respectively, from the corresponding p orbitals of carbon atoms. The higher energy blue-shifted bands correspond mostly to the π → π* transitions from the HOMO−1/−2 to LUMO+1/+2 located on the indenyl moieties.

In the (*Z*)-{BisIndSB}H_2 isomer, the LUMO orbital is also localized on the stilbene platform (82%), while the compositions of the HOMO−1 and HOMO−2 comprise only 29% and 59%, respectively, of the p orbitals of the diaryl-ethene fragment and mostly involve the contribution from the π-systems of the indenyl substituents. Thus, the lower and higher energy absorption bands for (*Z*)-{BisIndSB}H_2 represent the π → π* excitations implicating both the stilbene platform and the indenyl fragments.

TD-DFT calculations performed for {*o*-(*E*/*Z*)-BisIndSB}(Zr$(NMe_2)_3)_2$ complexes also returned results in good agreement with the experimental observations (Fig. S38†): for the (*E*)-

Table 1 UV-Vis absorption data (experimental and TD-DFT calculated), oscillator strengths *f* (larger than 0.2), main transitions and HOMO–LUMO gaps for proligands {*o*-(*E*/*Z*)-BisIndSB}H_2 and for complexes {*o*-(*E*/*Z*)-BisIndSB}$(Zr(NMe_2)_3)_2$ [a]

Compound	λ_{max} [nm] Exp.	Calc.	Oscillator strength *f*	Main transitions (weight)	E_{HOMO} [eV]	E_{LUMO} [eV]	HOMO–LUMO gap [eV]
{*o*-(*E*)-BisIndSB}H_2	305[b]	330[b]	0.8657	HOMO → LUMO	−6.00	−1.59	4.41
	257[b]	264[b]	0.3444	HOMO → LUMO+2 (32%) HOMO → LUMO+4 (15%) HOMO−4 → LUMO (15%)			
		256[b]	0.5341	HOMO−2 → LUMO+1 (40%) HOMO−1 → LUMO+2 (31%)			
{*o*-(*Z*)-BisIndSB}H_2	310[b]	319[b]	0.5806	HOMO → LUMO (93%)	−5.97	−1.36	4.61
	257[b]	258[b]	0.6552	HOMO−1 → LUMO+2 (35%) HOMO−2 → LUMO+1 (31%)			
{*o*-(*E*)-BisIndSB}$(Zr(NMe_2)_3)_2$	294[c]	362[c]	0.3680	HOMO−2 → LUMO (26%) HOMO → LUMO (62%)	−5.33[b]	−1.31[b]	4.02[b]
		356[c]	0.4700	HOMO−2 → LUMO (66%) HOMO → LUMO (18%)			
		311[c]	0.3282	HOMO−4 → LUMO (49%) HOMO−8 → LUMO (27%)			
{*o*-(*Z*)-BisIndSB}$(Zr(NMe_2)_3)_2$	293[c]	341[c]	0.4942	HOMO−2 → LUMO (88%)	−5.33[b]	−1.18[b]	4.15[b]
		305[c]	0.2584	HOMO−8 → LUMO (64%) HOMO−4 → LUMO (24%)			

[a] PBE0/def2-SVP, SCRF(SMD); see the ESI† for the details of TD-DFT calculations. [b] In CH_2Cl_2. [c] In toluene.

isomer, three major energy transitions at λ = 362, 356 and 311 nm, and two energy transitions at λ = 341 and 305 nm for the (*Z*)-isomer. In both molecules, the LUMO orbitals are represented, respectively, by the π*-systems of the *trans*- and *cis*-stilbene platforms with corresponding 81% and 83% contributions. The HOMO−1 and HOMO−2 in {*o*-(*E*/*Z*)-BisIndSB}$(Zr(NMe_2)_3)_2$ principally participate in the excitations to LUMO (red-shifted absorption bands at λ = 362/356 and 341 nm, respectively). They are notably localized on the nitrogen atoms of the Zr-amido groups (p(N) HOMO of 63% and 66%, respectively), and on the indenyl ligands (π-indenyl HOMO−2 of 57% and 56%, respectively). The higher-energy transitions, represented by absorption bands at λ = 311 and 305 nm, correspond to the excitations from the mixed p(N)/π-stilbene HOMO−4 and HOMO−8 to the π*-stilbene LUMO.

These unpretentious TD-DFT investigations, carried out for the stilbene platform-based molecules of neutral indene proligands and indenyl Zr-amido complexes derived thereof, revealed the participation of the π-systems of the indenyl fragments (neutral and anionic) and p(N) orbitals of the Zr-amido groups in the electronic transitions determining the principal absorption bands, which were observed experimentally. These results may suggest that the photo-induced degradation of the titled compounds under wavelength-selective irradiation could originate from undesired side reactions induced by the corresponding excitations. A more detailed analysis of the excited states could be more enlightening in addressing the nature of the degradation processes, which is yet beyond the scope of this study.

Polymerization studies. The dinuclear complexes {*m*/*p*-(*E*/*Z*)-BisIndSB}$(ZrCl_2Cp^*)_2$ and {*o*-(*E*/*Z*)-BisIndSB}$(Zr(NMe_2)_3)_2$, in combination with MAO, were explored in homogeneous homopolymerization of ethylene and 1-hexene, and in ethylene/1-hexene copolymerization (toluene solution, 5 bar ethylene constant pressure, T_{pol} = 50 °C).[31] For comparison purposes and to probe putative cooperativity effects in dinuclear active species, the catalytic performance of the mononuclear reference metallocene catalysts {(2-Me-4-Ph-Ind)(C_5Me_5)}$ZrCl_2$ (**mono-1**) and {(2-Me-4-Ph-Ind)}$Zr(NMe_2)_3$ (**mono-2**) were determined under identical conditions. Selected polymerization data are summarized in Tables S2–S6 (see the ESI†).

In homopolymerization of ethylene (Tables S2 and S5†) and in ethylene/1-hexene copolymerization (Tables S4 and S6†), both the mono- and dinuclear catalytic systems exhibited quite similar outcomes in terms of productivity, melting (T_m) and crystallization (T_c) transitions and molecular weight characteristics (M_n, M_w and D_M). Also, no significant differences between the above productivity/thermal/molecular property parameters were observed for the polymers produced from the *E*- and *Z*-isomers of the respective series of dinuclear catalysts. These observations suggest the absence of putative cooperativity phenomena within these dinuclear systems, at least under the reaction conditions investigated, which otherwise might affect positively on the chain growth process (at least, with the (*Z*)-isomers featuring closer distances between the two metal centers). This also indicates no significantly differentiated behavior between the (*Z*)- and (*E*)-isomers of a given type of complexes, reflecting either essentially similar intrinsic behavior or rapid interconversion (and hence averaged catalytic performance) of the respective active species under the reaction conditions.

In homopolymerization of 1-hexene (Table S3†), the dinuclear complexes unexpectedly appeared to be at least twice less productive with respect to the mononuclear reference catalyst

mono-1, however, still providing polymers with comparable molecular weight characteristics.

Conclusions

In the recent decades, considerable efforts have been made to introduce innovative concepts for the development of molecular polymerization catalysts enabling the design and customization of novel macromolecular architectures with tailored properties. Among the various families of catalysts envisioned, molecules with switchable platforms represent a fascinating and specialized area, allowing possible changes in their catalytic properties or reactivity in response to specific stimuli. In our contribution, we reported novel (*E*/*Z*)-stilbene-bridged ligand systems and a family of dinuclear group 4 metal complexes derived thereof, which constitute potential prototypes of light-responsive olefin polymerization catalysts. (*E*) ⇄ (*Z*)-photoisomerization of both proligands and complexes could be realized, however, eventually resulting in photo-induced decomposition. Theoretical methods (TD-DFT) may constitute a useful tool for understanding the origin of decomposition of the complexes in relation with the UV-Vis light absorption properties. In particular, the participation of the metal/ligand-localized orbitals in the principal transitions responsible for the (*E*) ⇄ (*Z*)-isomerization could trigger degradation processes. Olefin homo- and copolymerization investigations conducted with some of the prepared dinuclear systems revealed catalytic performance and polymer characteristics similar to those of structurally-related reference mononuclear complexes; this suggests the absence of putative cooperativity phenomena within these dinuclear systems and of significantly differentiated behavior between the (*Z*)- and (*E*)-isomers of a given type of complexes, at least under the reaction conditions investigated. Yet, these synthetic, spectroscopic and preliminary reactivity results shall be useful for the elaboration of more stable stimuli-switchable and more efficient polynuclear polymerization precatalysts with improved performances.

Experimental section

General considerations

All experiments involving air-sensitive compounds were performed under a dry argon atmosphere, using a glovebox or standard Schlenk techniques, unless otherwise stated. THF was freshly distilled from sodium benzophenone ketyl before use. Et_2O, pentane, dichloromethane and toluene were dried over alumina columns (MBraun system) and degassed by bubbling argon before use. Deuterated solvents (benzene-d_6, THF-d_8, chloroform-d_3, dichloromethane-d_2) were vacuum-distilled and stored on 3 Å molecular sieves. Cp*$ZrCl_3$, $TiCl_4$ and Zr$(NMe_2)_4$ were purchased from Strem Chemicals and used as received. $ZnCl_2$ was purified by refluxing in $SOCl_2$ and then dried under vacuum. MAO (30 wt% solution in toluene, Albemarle; contains *ca.* 10 wt% of free $AlMe_3$) was used as received. (*Z*)- and (*E*)-3,3′-dibromostilbene[23,24] and (*Z*)- and (*E*)-4,4′-dibromostilbene[26] were prepared following literature procedures. Single crystals of (*E*)-3,3′-dibromostilbene suitable for X-Ray diffraction analysis were obtained by recrystallization after adding pentane to a concentrated THF solution.

Instruments and measurements

NMR spectra were recorded on Bruker AM-400 and AM-500 spectrometers in Teflon-valved NMR tubes for long experiments or in normal NMR tubes with rubber septa for short experiments at room temperature. ^1H and ^{13}C NMR spectroscopy chemical shifts are reported in ppm *vs.* $SiMe_4$ and were determined using residual solvent signals. Assignment of signals was carried out using 1D (^1H, $^{13}C\{^1H\}$, JMOD) and 2D (COSY, HMBC, HSQC) NMR experiments. Coupling constants are given in hertz. Reliable and reproducible elemental analysis could not be obtained for the metal complexes, most probably due to their very high moisture-sensitivity. Inert Atmospheric Solid Analysis Probe (iASAP) was performed on a hybrid quadrupole time-of-flight mass spectrometer (Synapt G2, Waters Corp. Wilmslow, UK) in positive atmospheric solid analysis probe (ASAP) mode (Corona voltage 4.0 kV, probe temperature 650 °C, source temperature 140 °C, desolvatation gas flow 1200 L h^{-1}).[28] UV irradiation was performed in a Rayonet RPR-100 apparatus.

DFT computations

The calculations were performed using the Gaussian 09[32] program employing B3PW91[33,34] and PBE0 functionals,[35] and using a standard split valence basis set def2-SVP.[36] The solvent effects (toluene or dichloromethane) were taken into account during all the calculations by means of the SMD model.[37] Frequency calculations were performed to confirm that the optimized geometry is at a minimum on the potential energy surface (zero imaginary frequencies). TD-DFT calculations were performed at the same level of theory using the previously optimized geometries with PBE0 functional. Molecular orbitals (MOs) are drawn at the isovalue of 0.02 using Molekel[38] while theoretical absorption spectra were plotted using Multiwfn,[39] the half-bandwidths for the Gaussian model being taken equal to 3000 cm^{-1}. Percentage compositions of molecular orbitals were analyzed using Multiwfn,[38] and natural orbital analysis was done with the NBO 5.0 program.[40]

(*E*)-2,2′-Dibromostilbene

This compound was prepared following a procedure adapted from literature.[25,26] Zinc dust (3.57 g, 54.6 mmol, 2.0 equiv.) was added to a solution of $TiCl_4$ (3.10 mL, 28.4 mmol, 1.05 equiv.) in THF (100 mL) at 0 °C. Then, a solution of 2-bromobenzaldehyde (5.00 g, 3.15 mL, 27.0 mmol, 1.0 equiv.) in THF (20 mL) was added and the mixture was refluxed for 15 h. The reaction mixture was poured into 1 M HCl (50 mL), and the product was extracted with *n*-hexane (3 × 40 mL), washed with water (50 mL), brine (50 mL), and dried over Na_2SO_4. The filtrate was evaporated to afford an off-white solid which was recrystallized in a 5 : 95 v/v toluene/ethanol mixture to afford

(*E*)-2,2′-dibromostilbene as white needles (8.70 g, 95%). ^{1}H NMR (400 MHz, $CDCl_3$, 25 °C): δ 7.73 (dd, J = 7.8, 1.7, 2H, ArH-3), 7.65–7.56 (m, 2H, CH), 7.41 (s, J = 1.9, 2H, C*H*═C*H*), 7.34 (td, J = 7.6, 1.3, 2H, CH), 7.15 (td, J = 7.7, 1.7, 2H, ArH-4). ^{13}C{^{1}H} NMR (101 MHz, $CDCl_3$, 25 °C): δ 137.0 (C_{quat}), 133.2 (CH), 130.3 (CH), 129.4 (CH), 127.8 (CH), 127.3 (C═C), 124.4 (C–Br).

(*Z*)-2,2′-Dibromostilbene

This compound was prepared following a procedure adapted from literature.[23,25,26] (2-Bromobenzyl)triphenylphosphonium (11.10 g, 21.7 mmol, 1.3 equiv.), 2-bromobenzaldehyde (3.11 g, 16.8 mmol, 1.0 equiv.) and 18-*crown*-6 (0.440 g, 1.67 mmol, 0.1 equiv.) were mixed in CH_2Cl_2 (40 mL). The solution was cooled down to −78 °C and then, freshly powdered KOH (2.42 g, 43.3 mmol, 2.6 equiv.) was added. The reaction mixture was stirred for 1.5 h at −78 °C and allowed to heat up to room temperature and then stirred for an additional 3 h at room temperature. The solids formed were filtered off and the filtrate was washed with saturated NH_4Cl (20 mL), dried over $MgSO_4$ and the solvent was removed under reduced pressure. The solid obtained was purified by flash column chromatography (hexane/AcOEt, 9 : 1 v/v) to afford (*Z*)-2,2′-dibromostilbene as a white solid (4.09 g, 72%). ^{1}H NMR (400 MHz, $CDCl_3$, 25 °C): δ 7.66–7.47 (m, 2H, ArH-3), 7.12–6.91 (m, 6H, CH), 6.79 (s, 2H, C*H*═C*H*). ^{13}C{^{1}H} NMR (101 MHz, $CDCl_3$, 25 °C): δ 137.1 (C_{quat}), 132.7 (CH), 131.1 (CH), 128.9 (CH), 127.1 (C═C), 124.2 (CBr).

{*o*-(*E*)-BisIndSB}H_2

To a solution of (*E*)-2,2′-dibromostilbene (0.634 g, 1.88 mmol, 1.0 equiv.) in THF (40 mL) at −78 °C, *n*BuLi (1.7 mL of a 2.34 M solution in hexanes, 3.97 mmol, 2.1 equiv.) was added. The color changed from yellow to orange. After 30 min, $ZnCl_2$ (0.567 g, 4.15 mmol, 2.2 equiv.) in THF (10 mL) was added at −78 °C; the solution turned colorless. The resulting mixture was left to reach room temperature and the solvent was removed under vacuum, to leave a white sticky solid. Then, an orange solution of 7-bromo-2-methyl-1*H*-indene (0.833 g, 3.97 mmol, 2.1 equiv.) and Pd(P*t*Bu$_3$)$_2$ (0.042 g, 2.5 mol%) in THF (20 mL) was added onto the solid previously obtained and the resulting mixture was stirred for 15 h at room temperature. The reaction mixture was diluted with ethyl acetate (40 mL), washed with H_2O (20 mL), brine (20 mL), dried over $MgSO_4$ and the volatiles were removed under vacuum. The resulting oily substance was purified by flash column chromatography (100% petroleum ether) to afford {*o*-(*E*)-BisIndSB}H_2 as a white solid (0.607 g, 71%). ^{1}H NMR (400 MHz, CD_2Cl_2, 25 °C): δ 7.41–7.33 (m, 2H, CH stilbene), 7.30–7.27 (m, 4H, CH indenyl), 7.25–7.20 (m, 6H, CH stilbene), 6.94 (dd, J = 4.9, 3.7, 2H, CH Ind), 6.82 (s, 2H, C*H*═C*H*), 6.56 (q, J = 1.6, 2H, 3-Ind, 3′ Ind), 3.06 (s, 4H, CH_2), 2.10 (s, 6H, Me). ^{13}C{^{1}H} NMR (101 MHz, $CDCl_3$, 25 °C): δ 146.7 (C_{quat}), 146.0 (C_{quat}), 142.3 (C_{quat}), 140.5 (C_{quat}), 136.4 (C_{quat}), 135.7 (C_{quat}), 129.9, 127.9 (C═C), 127.6, 127.3, 127.2, 126.6, 125.5, 125.4, 119.1, 42.5 (*C*H$_2$), 16.9 (CH$_3$). ESI-MS: m/z calcd for $C_{34}H_{28}$ $[M]^+$: 437.2225; found: 437.2220.

{*o*-(*Z*)-BisIndSB}H_2

The synthesis was carried out following the same synthetic procedure as that described above for {*o*-(*E*)-BisIndSB}H_2 starting from (*Z*)-2,2′-dibromostilbene (0.600 g, 1.37 mmol). {*o*-(*Z*)-BisIndSB}H_2 was recovered as a white crystalline powder (0.525 g, 68%). ^{1}H NMR (400 MHz, CD_2Cl_2, 25 °C): δ 7.43–7.35 (m, 2H, CH stilbene), 7.33–7.23 (m, 4H, CH Ind), 7.23–7.11 (m, 6H, CH stilbene), 6.80 (dd, J = 6.8, 1.8, 2H, 5-Ind, 5′-Ind), 6.52 (q, J = 1.6, 2H, 3-Ind, 3′-Ind), 6.14 (s, 2H, C*H*═C*H*), 3.11 (s, 4H, CH_2), 2.1 (d, J = 1.4, 6H, Me). ^{13}C{^{1}H} NMR (101 MHz, CD_2Cl_2, 25 °C): δ 147.1 (C_{quat}), 146.4 (C_{quat}), 142.4 (C_{quat}), 141.4 (C_{quat}), 137.0 (C_{quat}), 136.0 (C_{quat}), 130.2, 130.7, 129.5, 127.4, 127.3, 127.2, 126.6, 125.6, 119.2, 42.6 (CH_2), 16.8 (CH_3). ESI-MS: m/z calcd for $C_{34}H_{28}$ $[M]^+$: 437.2225; found: 437.2224.

General procedure for synthesis of {*o*/*m*/*p*-(*E*/*Z*)-BisIndSB}(ZrCl$_2$Cp*)$_2$ complexes by Negishi coupling between *o*/*m*/*p*-(*E*/*Z*)-dibromostilbenes and (Cp*)(2-Me-4-Br-Ind)ZrCl$_2$

To a solution of brominated stilbene (1.0 equiv.) in THF (10 mL) at −80 °C, *n*BuLi (2.1 equiv., as a 2.5 M solution in hexanes) was added. The color turned immediately to yellow. After *ca.* 2–3 min, $ZnCl_2$ (2.1 equiv.) in THF (10 mL) was added at −78 °C, and the solution turned colorless. The mixture was stirred from −80 °C to room temperature and volatiles were removed under vacuum to obtain a white sticky solid. A colorless solution of (η^5-pentamethylcyclopentadienyl) (η^5-2-methyl-4-bromo-indenyl)$ZrCl_2$ (2.0 equiv.) and Pd(P*t*Bu$_3$)$_2$ (5 mol%) in THF (20 mL) was added to the white sticky solid and the mixture was stirred for 4 h at room temperature. Volatiles were pumped off, the orange oil obtained was solubilized in toluene and filtered over Celite. Addition of a few drops of pentane resulted in the precipitation of a black solid that was filtered off and discarded. The clear solution was evaporated under vacuum and the resulting solid was recrystallized several times in a toluene/pentane mixture (1 : 1 v/v) until a yellow crystalline solid was obtained.

{*m*-(*E*)-BisIndSB}(ZrCp*Cl$_2$)$_2$

The synthesis was conducted following the general Negishi coupling synthetic procedure described above starting from (*E*)-3,3′-dibromostilbene. The solid residue was recrystallized several times in a toluene/pentane (50 : 50 v/v) mixture offering {*m*-(*E*)-BisIndSB}(ZrCp*Cl$_2$)$_2$ as a yellow crystalline solid (0.350 g, 66%). ^{1}H NMR (400 MHz, C_6D_6, 25 °C): δ 7.41 (d, J = 7.3, 2H), 7.02 (d, J = 8.6, 2H), 6.84 (d, J = 2.4, 2H), 6.59 (t, J = 7.8, 2H), 5.69 (d, J = 2.4, 2H), 2.03 (s, 6H), 1.83 (s, 30H). ^{1}H NMR (500 MHz, $CDCl_3$, 25 °C): δ 7.53 (d, J = 7.1, 2H), 7.45 (d, J = 7.2, 2H), 7.35 (d, J = 8.2, 2H), 6.94–6.86 (m, 2H), 6.65 (s, 2H), 6.18 (t, J = 2.8, 2H), 2.24 (d, J = 3.1, 6H, Me-Ind), 2.01 (d, J = 2.5, 30H, Cp*). ^{1}H NMR (400 MHz, CD_2Cl_2, 25 °C): δ 7.96 (s, 2H), 7.59 (s, 2H), 7.54 (d, J = 8.3, 1H), 7.47 (d, J = 7.3, 1H), 7.35 (dt, J = 14.4, 7.8, 4H), 7.15 (q, J = 7.6, 4H), 6.81 (s, 2H), 6.27 (s, 2H), 2.21 (s, 6H), 2.03 (s, 30H). ^{13}C{^{1}H} NMR (101 MHz,

CD_2Cl_2, 25 °C): δ 126.57, 127.65, 126.19, 128.78, 121.22, 125.27, 128.77, 125.20, 114.45, 100.73, 15.66, 12.17. $^{13}C\{^1H\}$ NMR (126 MHz, $CDCl_3$, 25 °C): δ 128.67, 128.24, 126.50, 125.13, 120.86, 112.70, 101.62, 16.36 and 12.61 (Me Cp*).

Attempted synthesis of {*m*-(*Z*)-BisIndSB}(ZrCp*Cl$_2$)$_2$

The synthesis was conducted following the general Negishi coupling synthetic procedure described above starting from (*Z*)-3,3′-dibromostilbene except that the reaction was carried out overnight. The metallocene was recovered as a yellow solid in 60% yield but NMR analysis revealed a mixture of (*Z*)- and (*E*)-{*m*-BisIndSB}(ZrCp*Cl_2)$_2$. ^1H NMR (500 MHz, C_6D_6, 25 °C) (mixture of (*Z*)- and (*E*)-isomers) (Fig. S15†): δ 7.89–7.82 (m, 2H), 7.36–7.27 (m, 2H), 7.27–7.17 (m, 2H), 7.04–6.94 (m, 4H), 6.94–6.86 (m, 2H), 6.82 (dd, J = 10.2 and 2.2, 2H), 6.59 (d, J = 2.0, 2H), 5.69 (dd, J = 37.2 and 2.3, 2H), 5.72–5.57 (m, 2H), 1.95 (s, 6H, Me), 1.79 (d, J = 1.8, 30H, Cp*). $^{13}C\{^1H\}$ NMR (126 MHz, C_6D_6, 25 °C): δ 141.90 (C_{quat}), 134.25 (C_{quat} indenyl), 130.07 (CH), 128.49 (CH), 125.86 (CH), 120.68 (CH), 118.32 (C_{quat} indenyl), 114.95 (CH), 125.42 (CH), 114.25 (CH), 130.77 (CH), 104.61 (C_{quat} indenyl), 100.34 (CH), 15.74 (CH_3), 12.42 (Me Cp*).

{*p*-(*E*)-BisIndSB}(ZrCp*Cl$_2$)$_2$

The synthesis was conducted following the general Negishi coupling synthetic procedure described above starting from (*E*)-4,4′-dibromostilbene, except for the recrystallization step that was carried out in dichloromethane/pentane. {*p*-(*E*)-BisIndSB}(ZrCp*Cl_2)$_2$ was obtained as a yellow solid in 40% yield. ^1H NMR (500 MHz, C_6D_6, 25 °C): δ 7.93 (dd, J = 8.3 and 3.9, 2H), 7.52–7.29 (m, 6H), 7.15–6.97 (m, 8H), 5.72 (dd, J = 4.8 and 2.3, 2H, (*E*) C*H*═CH stilbene), 1.98 (d, J = 5.4, 6H, CH_3), 1.85–1.82 (m, 30H, Cp*). $^{13}C\{^1H\}$ NMR (126 MHz, C_6D_6, 25 °C): δ 139.21 (C_{quat} indenyl), 136.21 (C_{quat} indenyl), 130.24 (C_{quat} indenyl), 129.28 (CH), 128.68 (CH), 126.96 (CH), 126.84 (CH), 125.49 (CH), 125.34 (CH), 120.60 (CH), 114.42 (CH), 100.43 ((*E*)-*C*H═CH stilbene), 114.68 (C_{quat}), 15.68 (CH_3), 12.40 (Cp*).

{*p*-(*Z*)-BisIndSB}(ZrCp*Cl$_2$)$_2$

The synthesis was conducted following the general Negishi coupling synthetic procedure described above starting from (*Z*)-4,4′-dibromostilbene. {*p*-(*Z*)-BisIndSB}(ZrCp*Cl_2)$_2$ was obtained as a bright yellow solid in 58% yield. ^1H NMR (500 MHz, C_6D_6, 25 °C): δ 7.81–7.70 (m, 2H, C*H*), 7.41 (d, J = 8.1, 2H, C*H*), 7.36–7.26 (m, 2H, C*H*), 7.26–7.18 (m, 2H, C*H*), 7.08–6.98 (m, 2H, C*H*), 6.98–6.85 (m, 4H, C*H*), 6.48 (dd, J = 5.2 and 2.8, 2H, C*H*), 5.76–5.65 (m, 2H, C*H*), 2.08 (d, J = 2.2, 6H, CH_3), 1.80 (d, J = 1.8, 30H, Cp*). $^{13}C\{^1H\}$ NMR (75 MHz, C_6D_6, 25 °C): δ 128.74 (*C*H), 129.13 (*C*H), 128.53 (*C*H), 125.50 (*C*H), 120.57 (*C*H), 124.97 (*C*H), 113.08 (*C*H), 130.08 (*C*H), 100.78 (*C*H), 13.10 (*C*H_3), 12.29 (Me Cp*).

General procedure for the synthesis of {*o*-(*E*/*Z*)-BisIndSB}(ZrCl$_2$Cp*)$_2$ using Cp*ZrCl$_3$

To a solution of {*o*-(*E*/*Z*)-BisIndSB}H_2 (1.0 equiv.) in toluene (10 mL) at −78 °C, *n*BuLi (2.1 equiv., as a 2.5 M solution in hexanes) was added. The resulting mixture was stirred for 40 h at RT and then added to a suspension of Cp*$ZrCl_3$ in toluene (10 mL). This mixture was then stirred for 40 h at 100 °C. The hot mixture was filtered through Celite and the filtrate was evaporated to dryness. The residue obtained was recrystallized several times in a toluene/pentane mixture until a yellow crystalline solid was obtained.

{*o*-(*E*)-BisIndSB}(Zr(NMe$_2$)$_3$)$_2$

In a Schlenk flask containing {*o*-(*E*)-BisIndSB}H_2 (0.150 g, 0.34 mmol, 1.0 equiv.) and Zr(NMe_2)$_4$ (0.184 g, 0.69 mmol, 2.0 equiv.), toluene (10 mL) was added. The resulting solution was heated at 70 °C for 36 h and, over this time period, volatiles were stripped every 3 h. Complete evaporation of volatiles and recrystallization of the resulting solid residue from a toluene/hexane (1 : 4 v/v) solution afforded {(*E*)-*o*-BisIndSt}(Zr(NMe_2)$_3$)$_2$ as a pale yellow crystalline solid (0.257 g, 86%). ^1H NMR (400 MHz, C_6D_6, 25 °C): δ 7.66–7.61 (m, 2H), 7.49–7.36 (m, 4H), 7.16–7.11 (m, 4H), 7.06–6.97 (m, 6H), 6.12–6.04 (s, 4H, CH indenyl), 2.76 (s, 36H, NMe_2), 2.14 (s, 6H, Me indenyl). $^{13}C\{^1H\}$ NMR (101 MHz, C_6D_6, 25 °C): δ 140.4 (C_{quat}), 136.7 (C_{quat}), 132.7 (C_{quat}), 130.2 (*C*H), 128.8, 128.4, 127.9, 127.4, 126.8 (C_{quat}), 126.6 (C_{quat}), 126.2, 125.7 (C_{quat}), 125.2, 125.0, 123.0, 121.6, 99.7 (*C*H Ind), 99.6 (*C*H Ind), 44.4 (NMe_2), 14.8 (*C*H_3 Ind). iASAP-MS: m/z calcd for $C_{46}H_{63}N_6Zr_2$ $[MH]^+$: 879.3208; found: 879.3208.

{*o*-(*Z*)-BisIndSB}(Zr(NMe$_2$)$_3$)$_2$

Using a similar protocol as that described above for {*o*-(*E*)-BisIndSB}(Zr(NMe_2)$_3$)$_2$, complex {*o*-(*Z*)-BisIndSB}(Zr(NMe_2)$_3$)$_2$ was synthetized from {*o*-(*Z*)-BisIndSB}H_2 (0.200 g, 0.453 mmol) and Zr(NMe_2)$_4$ (0.245 mg, 0.918 mmol, 2 equiv.). Recrystallization of the crude product from a toluene/hexane (1 : 4 v/v) solution afforded {*o*-(*Z*)-BisIndSB}(Zr(NMe_2)$_3$)$_2$ as a pale yellow crystalline solid (0.353 g, 78%). ^1H NMR (400 MHz, C_6D_6, 25 °C): δ 7.78–7.68 (m, 4H), 7.43–7.39 (m, 2H), 7.24–7.2 (m, 2H), 7.08–7.02 (m, 6H), 6.42–6.36 (m, 2H), 6.1–6.07 (m, 4H, CH indenyl), 2.75 (s, 36H, NMe_2), 2.12, (s, 6H, Me indenyl). $^{13}C\{^1H\}$ NMR (100 MHz, C_6D_6, 25 °C): δ 141.0 (C_{quat}), 136.8 (C_{quat}), 134.6 (C_{quat}), 132.5 (C_{quat}), 130.5 (C_{quat}), 130.4 (C_{quat}), 130.3, 130.0, 127.3, 127.2, 126.2, 125.2, 125.0, 123.0, 121.6, 99.4 (*C*H Ind), 99.3 (*C*H Ind), 44.4 (NMe_2), 14.8 (*C*H_3 Ind). iASAP-MS: m/z calcd for $C_{46}H_{63}N_6Zr_2$ $[MH]^+$: 879.3208; found: 879.3209.

Author contributions

N. R. and T. C. designed and performed the experimental work. T. R. conducted the crystallographic studies. A. W. cosupervized the work and contributed to evolution of the initial project. E. K. conducted the DFT studies. J. F. C. wrote the initial draft. E. K., N. R. and J. F. C. revised the final manuscript. E. K. and J. F. C. directed the research. All authors contributed to the various sections of the manuscript.

Conflicts of interest

Some of the authors have filled a related patent application: A. Welle, A. Vantomme, J.-F. Carpentier, N. Romero, E. Kirillov (Univ. Rennes 1, CNRS and Total), *Eur. Pat. Appl.* 17 306 163.1 (08/09/2017); *WO Pat.* 2019 048561 (06/09/2018).

Acknowledgements

This work was financially supported by TotalEnergies (post-doctoral fellowships to NR and TC). We gratefully thank Philippe Jehan for MS analyses. Part of this work has been performed using mass and NMR spectrometers belonging to the CRMPO (UAR ScanMAT, CNRS-Université de Rennes) core facility. We thank Prof. Stéphane Rigaut for fruitful discussions re. UV-vis spectroscopy.

References

1 (*a*) *Molecular switches*, ed. B. L. Feringa and W. R. Browne, Wiley VCH, 2nd edn, 2012; (*b*) M. Natali and S. Giordani, Molecular switches as photocontrollable "smart" receptors, *Chem. Soc. Rev.*, 2012, **41**, 4010–4029.

2 V. Blanco, D. A. Leigh and V. Marcos, Artificial switchable catalysts, *Chem. Soc. Rev.*, 2015, **44**, 5341–5370.

3 (*a*) F. A. Leibfarth, K. M. Mattson, B. P. Fors, H. A. Collins and C. J. Hawker, External regulation of controlled polymerizations, *Angew. Chem., Int. Ed.*, 2013, **52**, 199–210; (*b*) A. J. Teator, D. N. Lastovickova and C. W. Bielawski, Switchable Polymerization Catalysts, *Chem. Rev.*, 2016, **116**, 1969–1992; (*c*) Q. Michaudel, V. Kottisch and B. P. Fors, Cationic polymerization: from photoinitiation to photocontrol, *Angew. Chem., Int. Ed.*, 2017, **56**, 9670–9679; (*d*) C. Chen, Redox-controlled polymerization and copolymerization, *ACS Catal.*, 2018, **8**, 5506–5514; (*e*) A. M. Doerr, J. M. Burroughs, S. R. Gitter, X. Yang, A. J. Boydston and B. K. Long, Advances in Polymerizations Modulated by External Stimuli, *ACS Catal.*, 2020, **10**, 14457–14515; (*f*) Y.-N. Zhou, J.-J. Li, Y.-Y. Wu and Z.-H. Luo, Role of External Field in Polymerization: Mechanism and Kinetics, *Chem. Rev.*, 2020, **120**, 2950–3048.

4 (*a*) K. Arumugam, C. D. Varnado, S. Sproules, V. M. Lynch and C. W. Bielawski, Redox–switchable ring–closing metathesis: Catalyst design, synthesis, and study, *Chem. – Eur. J.*, 2013, **19**, 10866–10875; (*b*) A. J. Teator, H. Shao, G. Lu, P. Liu and C. W. Bielawski, A photoswitchable olefin metathesis catalyst, *Organometallics*, 2017, **36**, 490–497.

5 A. J. D. Magenau, N. C. Strandwitz, A. Gennaro and K. Matyjaszewski, Electrochemically mediated atom transfer radical polymerization, *Science*, 2011, **332**, 81–84.

6 C. K. A. Gregson, V. C. Gibson, N. J. Long, E. L. Marshall, P. J. Oxford and A. J. P. White, Redox control within single-site polymerization catalysts, *J. Am. Chem. Soc.*, 2006, **128**, 7410–7411.

7 (*a*) E. M. Broderick, N. Guo, C. S. Vogel, C. Xu, J. Sutter, J. T. Miller, K. Meyer, P. Mehrkhodavandi and P. L. Diaconescu, Redox control of a ring-opening polymerization catalyst, *J. Am. Chem. Soc.*, 2011, **133**, 9278–9281; (*b*) E. M. Broderick, N. Guo, T. Wu, C. S. Vogel, C. Xu, J. Sutter, J. T. Miller, T. Cantat and P. L. Diaconescu, Redox control of a polymerization catalyst by changing the oxidation state of the metal center, *Chem. Commun.*, 2011, **47**, 9897–9899; (*c*) E. M. Broderick, P. S. Thuy-Boun, N. Guo, C. S. Vogel, J. Sutter, J. T. Miller, K. Meyer and P. L. Diaconescu, Synthesis and characterization of cerium and yttrium alkoxide complexes supported by ferrocene-based chelating ligands, *Inorg. Chem.*, 2011, **50**, 2870–2877; (*d*) X. Wang, A. Thevenon, J. L. Brosmer, I. Yu, S. I. Khan, P. Mehrkhodavandi and P. L. Diaconescu, Redox control of group 4 metal ring-opening polymerization activity toward l-lactide and ε-caprolactone, *J. Am. Chem. Soc.*, 2014, **136**, 11264–11267; (*e*) J. Wei, M. N. Riffel and P. L. Diaconescu, Redox control of aluminum ring-opening polymerization: a combined experimental and DFT investigation, *Macromolecules*, 2017, **50**, 1847–1861; (*f*) S. M. Quan, J. Wei and P. L. Diaconescu, Mechanistic studies of redox-switchable copolymerization of lactide and cyclohexene oxide by a zirconium complex, *Organometallics*, 2017, **36**, 4451–4457; (*g*) J. Wei and P. L. Diaconescu, Redox-switchable ring-opening polymerization with ferrocene derivatives, *Acc. Chem. Res.*, 2019, **52**, 415–424.

8 M. Li, P. Zhang and C. Chen, Light-controlled switchable ring-opening polymerization, *Macromolecules*, 2019, **52**, 5646–5651.

9 A. Sauer, J. C. Buffet, T. P. Spaniol, H. Nagae, K. Mashima and J. Okuda, Switching the lactide polymerization activity of a cerium complex by redox reactions, *ChemCatChem*, 2013, **5**, 1088–1091.

10 A. B. Biernesser, B. Li and J. A. Byers, Redox-controlled polymerization of lactide catalyzed by bis (imino) pyridine iron bis(alkoxide) complexes, *J. Am. Chem. Soc.*, 2013, **135**, 16553–16560.

11 Y.-Y. Fang, W.-J. Gong, X.-J. Shang, H.-X. Li, J. Gao and J. P. Lang, Synthesis and structure of a ferric complex of 2, 6-di(1*H*-pyrazol-3-yl) pyridine and its excellent performance in the redox-controlled living ring-opening polymerization of ε-caprolactone, *Dalton Trans.*, 2014, **43**, 8282–8289.

12 H. J. Yoon, J. Kuwabara, J. H. Kim and C. A. Mirkin, Allosteric supramolecular triple-layer catalysts, *Science*, 2010, **330**, 66–69.

13 B. M. Neilson and C. W. Bielawski, Photoswitchable NHC-promoted ring-opening polymerizations, *Chem. Commun.*, 2013, **49**, 5453–5455.

14 (*a*) M. Zhao and C. Chen, Accessing multiple catalytically active states in redox-controlled olefin polymerization, *ACS Catal.*, 2017, **7**, 7490–7494; (*b*) D. Peng and C. Chen, Photoresponsive palladium and nickel catalysts for ethylene polymerization and copolymerization, *Angew. Chem., Int. Ed.*, 2021, **60**, 22195–22200; (*c*) W. C. Anderson, S. H. Park, L. A. Brown, J. M. Kaisera and B. K. Long,

Accessing multiple polyethylene grades via a single redox-active olefin polymerization catalyst, *Inorg. Chem. Front.*, 2017, **4**, 1108–1112; (*d*) Z. Liu, Y. Gong, J. Zhang, S. Liu and Z. Li, Dinuclear half-titanocene complex bearing an anthracene-bridged bifunctional alkoxide ligand: Unprecedented cooperativity toward copolymerization of ethylene with 1-octene or norbornene, *Macromolecules*, 2024, **57**, 162–173.

15 R. Maity, B. S. Birenheide, F. Breher and B. Sarkar, Cooperative effects in multimetallic complexes applied in catalysis, *ChemCatChem*, 2021, **13**, 2337–2370.

16 (*a*) M. Delferro and T. J. Marks, Multinuclear olefin polymerization catalysts, *Chem. Rev.*, 2011, **111**, 2450–2485; (*b*) J. P. McInnis, M. Delferro and T. J. Marks, Multinuclear Group 4 catalysis: Olefin polymerization pathways modified by strong metal–metal cooperative effects, *Acc. Chem. Res.*, 2014, **47**, 2545–2557; (*c*) Y. Gao, A. R. Mouat, A. Motta, A. Macchioni, C. Zuccaccia, M. Delferro and T. J. Marks, Pyridylamido bi-hafnium olefin polymerization catalysis: Conformationally supported Hf···Hf enchainment cooperativity, *ACS Catal.*, 2015, **5**, 5272–5282.

17 S. Jüngling, R. Müllhaupt and H. Plenio, Cooperative effects in binuclear zirconocenes: Their synthesis and use as catalyst in propene polymerization, *J. Organomet. Chem.*, 1993, **460**, 191–195.

18 X. Yan, A. Chernega, M. L. H. Green, J. Sanders, J. Souter and T. Ushioda, Proximity and cooperativity effects in binuclear d^0 olefin polymerization catalysis. Theoretical analysis of structure and reaction mechanism, *J. Mol. Catal. A: Chem.*, 1998, **128**, 119–141.

19 L. N. Jende, T. Roisnel, V. Cirriez, A. Welle, E. Kirillov and J.-F. Carpentier, An asymmetric dinuclear bis(*ansa*-zirconocene) complex: Synthesis and performance in olefin (co-) polymerization, *Catalysts*, 2023, **13**, 1108 and references cited therein.

20 T. Nevesely, M. Wienhold, J. J. Molloy and R. Gilmour, Advances in the E⇄*Z* isomerization of alkenes using small molecule photocatalysts, *Chem. Rev.*, 2022, **122**, 2650–2694.

21 Similar calculations of ΔG_{298} values for the {*o*-(*E*/*Z*)-BisIndSB}H_2 proligand platform also corroborated the higher stability of the (*E*)-isomer with respect to the (*Z*)-counterpart by 6.4 kcal mol^{-1}.

22 J. Saltiel, A. Marinari, D. W. L. Chang, J. C. Mitchener and E. D. Megarity, *Trans-cis* photoisomerization of the stilbenes and a reexamination of the positional dependence of the heavy-atom effect, *J. Am. Chem. Soc.*, 1979, **101**, 2982–2996.

23 M. Oba, M. Iida, T. Nagoya and K. Nishiyama, Synthesis of a novel silicon-bridged [2.2]metacyclophan-9-ene and its photolytic transannular reaction, *J. Organomet. Chem.*, 2006, **691**, 1151–1153.

24 P. Beak and C. Liu, Evidence for bromine-lithium exchange in a local high concentration gradient, *Tetrahedron*, 1994, **50**, 5999–6004.

25 H.-G. Imrich, J. Conrad and U. Beifuss, Copper-catalyzed double Intramolecular Ullmann coupling for the synthesis of diastereomerically and enantiomerically pure 4b,9b-dihydrobenzofuro-[3,2-*b*]benzofurans, *Eur. J. Org. Chem.*, 2015, 7718–7734.

26 M. Linseis, S. Záliš, M. Zabel and R. F. Winter, Ruthenium stilbenyl and diruthenium distyrylethene complexes: Aspects of electron delocalization and electrocatalyzed isomerization of the *Z*-isomer, *J. Am. Chem. Soc.*, 2012, **134**, 16671–16692.

27 V. V. Izmer, A. Y. Lebedev, M. V. Nikulin, A. N. Ryabov, A. F. Asachenko, A. V. Lygin, D. A. Sorokin and A. Z. Voskoboynikov, *ansa*-zirconocene catalysts for isotactic-selective propene polymerization at high temperature: A long story finds a happy ending, *Organometallics*, 2006, **25**, 1217–1229.

28 A. Naim, M. Farenc, M. Hubert-Roux, T. Chavagnan, V. Cirriez, A. Welle, A. Vantomme, E. Kirillov, J.-F. Carpentier, C. Afonso and P. Giusti, Paraffin-Inert Atmospheric Solid Analysis probe (piASAP): A fast and easy approach to characterize extremely air-sensitive organometallic complexes by mass spectrometry, *Anal. Chem.*, 2020, **92**, 2922–2925.

29 G. S. Hammond, J. Saltiel, A. A. Lamola, N. J. Turro, J. S. Bradshaw, D. O. Cowan, R. C. Counsell, V. Vogt and C. Dalton, Mechanisms of photochemical reactions in solution. XXII.1 Photochemical cis-trans isomerization, *J. Am. Chem. Soc.*, 1964, **86**, 3197–3217.

30 For *ab initio* calculations of molecular systems based on stilbene platforms, see: (*a*) Ref. 26; (*b*) P. Pal, S. Mukherjee, D. Maity and S. Baitalik, Synthesis, structural characterization, and luminescence switching of diarylethene-conjugated Ru(II)-terpyridine complexes by trans-cis photoisomerization: experimental and DFT/TD-DFT investigation, *Inorg. Chem.*, 2018, **57**, 5743–5753; (*c*) R. Improta and F. Santoro, Excited-state behavior of *trans* and *cis* isomers of stilbene and stiff stilbene: a TD-DFT study, *J. Phys. Chem. A*, 2005, **109**, 10058–10067; (*d*) D. L. Beveridge and H. H. Jaffe, The electronic structure and spectra of cis- and trans-stilbene, *J. Am. Chem. Soc.*, 1965, **87**, 5340–5346.

31 Each polymerization experiment was independently repeated twice under the same conditions, revealing acceptable (±1 (0%) reproducibility in terms of productivity and physicochemical properties of the isolated polymer; duplicated experiments are provided in Tables S2–S6 (see the ESI†).

32 M. J. Frisch, G. W. Trucks, H. B. Schlegel, G. E. Scuseria, M. A. Robb, J. R. Cheeseman, G. Scalmani, V. Barone, B. Mennucci, G. A. Petersson, H. Nakatsuji, M. Caricato, X. Li, H. P. Hratchian, A. F. Izmaylov, J. Bloino, G. Zheng, J. L. Sonnenberg, M. Hada, M. Ehara, K. Toyota, R. Fukuda, J. Hasegawa, M. Ishida, T. Nakajima, Y. Honda, O. Kitao, H. Nakai, T. Vreven, J. A. Montgomery Jr., J. E. Peralta, F. Ogliaro, M. Bearpark, J. J. Heyd, E. Brothers, K. N. Kudin, V. N. Staroverov, R. Kobayashi, J. Normand, K. Raghavachari, A. Rendell, J. C. Burant, S. S. Iyengar, J. Tomasi, M. Cossi, N. Rega, J. M. Millam, M. Klene, J. E. Knox, J. B. Cross, V. Bakken, C. Adamo, J. Jaramillo, R. Gomperts, R. E. Stratmann, O. Yazyev, A. J. Austin,

R. Cammi, C. Pomelli, J. W. Ochterski, R. L. Martin, K. Morokuma, V. G. Zakrzewski, G. A. Voth, P. Salvador, J. J. Dannenberg, S. Dapprich, A. D. Daniels, Ö. Farkas, J. B. Foresman, J. V. Ortiz, J. Cioslowski and D. J. Fox, *Gaussian 09, Revision D.01*, Gaussian Inc., Pittsburgh, PA, 2009.

33 A. D. Becke, Density-Functional exchange-energy approximation with correct asymptotic behavior, *Phys. Rev. A*, 1988, **38**, 3098–3100.

34 A. D. Becke, Density-functional thermochemistry. III. The role of exact exchange, *J. Chem. Phys.*, 1993, **98**, 5648–5652.

35 C. Adamo and V. Barone, Toward reliable density functional methods without adjustable parameters: The PBE0 model, *J. Chem. Phys.*, 1999, **110**, 6158–6169.

36 F. Weigend and R. Ahlrichs, Balanced basis sets of split valence, triple zeta valence and quadruple zeta valence quality for H to Rn: Design and assessment of accuracy, *Phys. Chem. Chem. Phys.*, 2005, **7**, 3297–3305.

37 A. V. Marenich, C. J. Cramer and D. G. Truhlar, Universal solvation model based on solute electron density and on a continuum model of the solvent defined by the bulk dielectric constant and atomic surface tensions, *J. Phys. Chem. B*, 2009, **113**, 6378–6396.

38 U. Varetto, *Molekel 5.4, an open-source multi-platform molecular visualization program*. **https://ugovaretto.github.io/molekel/wiki/pmwiki.php/Main/HomePage.html**.

39 T. Lu and F. Chen, Multiwfn: A multifunctional wavefunction analyzer, *J. Comput. Chem.*, 2012, **33**, 580–592.

40 E. D. Glendening, J. K. Badenhoop, A. E. Reed, J. E. Carpenter, J. A. Bohmann, C. M. Morales and F. Weinhold, *NBO 5.0*, Theoretical Chemistry Institute, University of Wisconsin, Madison, WI, 2001; **https://www.chem.wisc.edu/nbo5**.